Title

Assembly and Pre-Loading Specifications for the Series Production of the Nb3Sn MQXFA Quadrupole Magnets for the HL-LHC

Journal

IEEE Transactions on Applied Superconductivity, 32(6)

ISSN

1051-8223

Authors

Ferracin, P

Ambrosio, G

Cheng, DW

et al.

Publication Date

2022

DOI

10.1109/tasc.2022.3148971

Assembly and Pre-Loading Specifications for the Series Production of the Nb_3Sn MQXFA Quadrupole Magnets for the HL-LHC

P. Ferracin, G. Ambrosio, D. W. Cheng, J. Ferradas Troitino, L. Garcia Fajardo, S. Izquierdo Bermudez, S. Prestemon, K. L. Ray, M. J. Solis, E. Todesco, and G. Vallone

***Abstract*—The High Luminosity LHC (HL-LHC) Project is planning to install 16 cold-masses made with Nb_3Sn quadrupole magnets in the LHC Interaction Regions to significantly increase its luminosity. Half of these cold masses are fabricated at BNL, FNAL, and LBNL under the US Accelerator Research Program (AUP). Each cold mass includes two identical Nb_3Sn quadrupole magnets, called MQXFA with a magnetic length of 4.2 m. Currently, the AUP project has completed the fabrication and test of the first 5 pre-series magnets, and is working on the following 16 magnets for the series production. The brittleness and strain sensitivity of the Nb_3Sn superconducting material requires a careful definition of the allowable maximum stress in the windings during magnet assembly and pre-load, and a tight control of their variation within the whole coil length. Therefore, a series of assembly and pre-load specifications have been defined with the goals of minimizing the risk of conductor degradation and providing the mechanical support required to reach the nominal current during powering. In this paper we present the specifications defined for the MQXFA magnets and applied during the different assembly phases and during the pre-load process of the first 5 pre-series magnets.**

***Index Terms*—High luminosity LHC, interaction regions, low-β quadrupoles, Nb_3Sn magnets.**

I. Introduction

THE US Accelerator Upgrade Program (AUP) [1] is in the process of fabricating 8 cold masses (plus 2 spares) to be installed in the LHC Interaction Regions as part of the High Luminosity LHC (HL-LHC) Project [2], [3]. Each cold mass will contain two superconducting quadrupole magnets, called MQXFA, with a magnetic length of 4.2 m and Nb_3Sn superconducting coils. In parallel, CERN is fabricating 8 cold masses (plus 2 spares), each featuring a single 7.15 m long magnet, called MQXFB with identical cross-section design as the US magnets [4], [5]. Since 2016, a total of six short models (MQXFS1, MQXFS3−7) and two long prototypes, for both the "A" magnets (MQXFAP1-2) and the "B" magnets (MQXFBP1-P2) have been fabricated and tested. In addition, at the time of the submission of this paper, 4 "pre-series magnets" MQXFA03-07 have been completed.

Pre-series magnets are deliverable magnets fabricated before finalizing series-magnet specifications. Test results are reported in [6]–[10]. Starting with magnet MQXFA03 in 2019, assembly and pre-load operations, performed at LBNL, were executed following a set of specifications aimed at guaranteeing a uniform and controlled stress in the brittle Nb_3Sn superconducting coils. In particular, dimensional acceptable values were defined on the sub-components of the mechanical structure, and maximum and target stress on the windings were established to minimize the risk of conductor degradation and, at the same time, to provide sufficient mechanical support to the coils during magnet operation. Such specifications derive from all the experience gained during the MQXF short model and prototype programs, both in Europe and in the US, and, previously, from the R&D performed by the US LHC Accelerator Research Program (LARP) [11], [12].

In this paper, after a brief description of the magnet design and of the assembly steps (Section II), we list the specifications for the assembly of the MQXFA magnet in Sections III and IV, and for the coil pre-load in Section V.

II. Magnet Design and Assembly Steps

The design and the assembly process of the MQXFA quadrupole magnet is described in detail in [13] and is shown schematically in Fig. 1. From left to right, the different phases of the assembly are represented. The shell-yoke sub-assembly (left) features four iron yoke stacks locked with four gap keys inside an aluminum shell. The coil-pack sub-assembly (center) includes four coils wound around a Ti-alloy winding pole, which includes a pole G10 key for alignment. The coils are surrounded by aluminum collars and bolted iron pads. The two sub-assemblies are combined in the magnet (right), where two trapezoidal master keys, containing two loading keys and one central alignment key, are inserted to provide room for the water pressurized bladders,

Manuscript received November 30, 2021; revised January 21, 2022; accepted January 31, 2022. Date of publication February 7, 2022; date of current version February 23, 2022. This work was supported in part by the U.S. Department of Energy, Office of Science, Office of High Energy Physics, in part by the US LHC Accelerator Research Program (LARP), and in part by the US LHC Accelerator Upgrade Project (AUP), and in part by the High Luminosity LHC project at CERN. (*Corresponding author: Paolo Ferracin.*)

P. Ferracin, D. W. Cheng, L. Garcia Fajardo, S. Prestemon, K. L. Ray, M. J. Solis, and G. Vallone are with the Lawrence Berkeley National Lab, Berkeley, CA 94720 USA (e-mail: pferracin@lbl.gov).

J. Ferradas Troitino, S. Izquierdo Bermudez, and E. Todesco are with the CERN, CH-1211 Geneva 23, Switzerland.

G. Ambrosio is with the Fermi National Accelerator Laboratory, Batavia, IL 80510 USA.

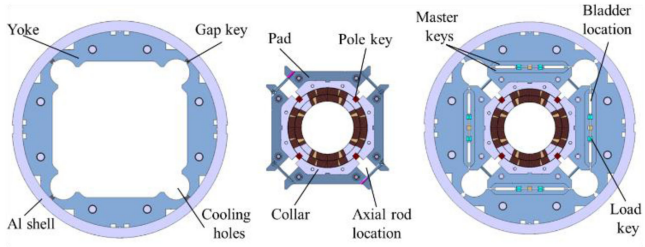

Fig. 1. The 3 steps of the MQXF magnet assembly: shell-yoke sub-assembly (left), coil-pack sub-assembly (center), and the magnet assembly (right).

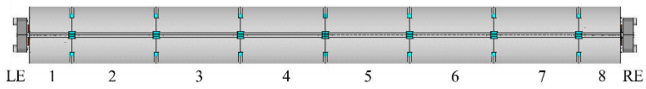

Fig. 2. 3D view of the MQXFA magnets, with shell segments 1 to 8, from lead end (LE, left) to return end (RE, right).

which are used to pre-compress the coil and pre-tension the shell. The 3D design, shown in Fig. 2, is characterized by 8 segmented aluminum shell and two end-plates. The end-plates are placed at the lead end (LE) and at the return end (RE), and are connected by 4 full length axial rods to provide axial support and pre-load to the coil ends.

To monitor the strain during all the operations, three shells (#2, #4, and #7) are instrumented with strain gauges measuring both in the axial and azimuthal direction in each quadrant. In addition, in all four coils, the winding poles are instrumented with azimuthal and axial strain gauges, in the axial location at the center of shell 7 (close to the RE). Finally, each axial rod is equipped with an axial strain gauge. It is important to point out that according to 2D FE analysis, the stress in the inner radius of the winding pole, where the strain gauges are mounted, is a good representation of the stress in the inner radius of the pole turn, where the coil peak stress is located [14].

III. Shell-Yoke Sub-Assembly

The assembly of the shell-yoke sub-assembly is performed by combining two half-length shell-yoke modules: the LE module, with shells 1 to 4, and the RE module, with shells 5 to 8. Each module is assembled vertically, by inserting the 4 yoke stacks inside the 4 shells. Once positioned inside the shells, the yoke stacks are spread apart and pushed against the shells by bladders placed in the 4 cooling holes (round cut-outs in the yokes), with a dedicated tooling. This pre-load operation produces a (relatively low) azimuthal tension in the shell. Four "gap keys" are then slid in between the yokes (radially close to the shell) to lock the pre-load before the deflation and extraction of the bladders. At this point the two sub-modules are placed horizontally and connected by tie rods to form the shell-yoke sub-assembly. The specifications related to this part of the assembly will be described in the next sub-sections.

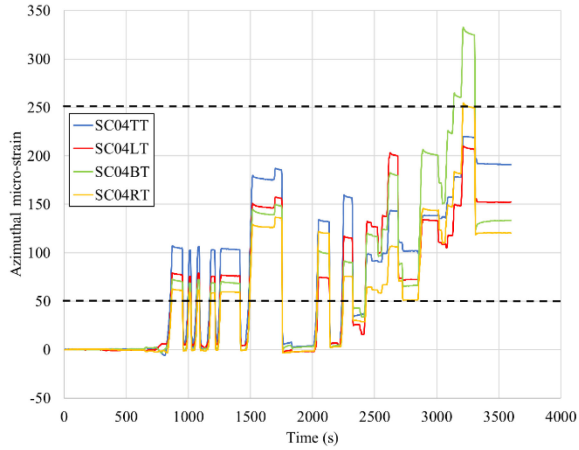

Fig. 3. Shell azimuthal micro-strain measured during bladder operation in the shell-yoke sub-assembly, in shell 4 of magnet MQXFA06; the dashed lines indicate the minimum and maximum values of the specifications.

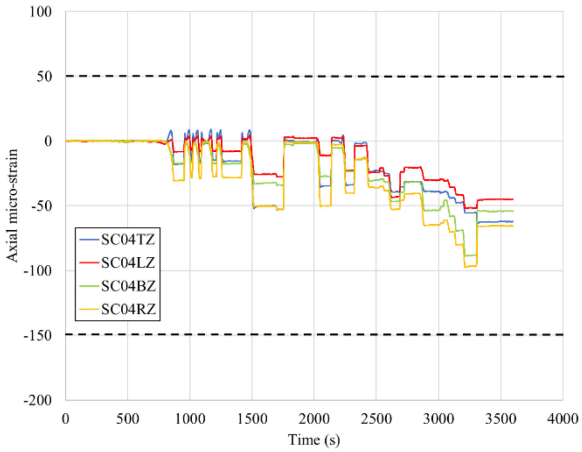

Fig. 4. Shell axial micro-strain measured during bladder operation in the shell-yoke sub-assembly, in shell 4 of magnet MQXFA06; the dashed lines indicate the minimum and maximum values of the specifications.

A. Shell Strain in Shell-Yoke Sub-Assembly

The nominal yoke gap, i.e., the gap between the yokes where the yoke keys are inserted, is 12 mm. The gap keys, inserted via the bladder inflation, are 12.1 mm thick. Therefore, the resulting interference produces azimuthal tension in the shells, which is measured by stain gauges. In Figs. 3 and 4, the shell azimuthal and axial micro-strain measured before and after the insertion of the gap keys are plotted for shell 4 in magnet MQXFA06. According to strain gauge measurements taken on short models, prototype magnets, and pre-series magnets, a 0.100 mm interference of the yoke key produces typically an average shell strain of about $+150$ micro-strain in the azimuthal direction, and of about -50 micro-strain in the axial direction, with variations of about ± 100 micro-strain. Therefore, for this operation, the following specifications are set:

- The shell strain in the azimuthal direction after shell-yoke sub-assembly shall be within $+0.050/+0.250$ micro-strain

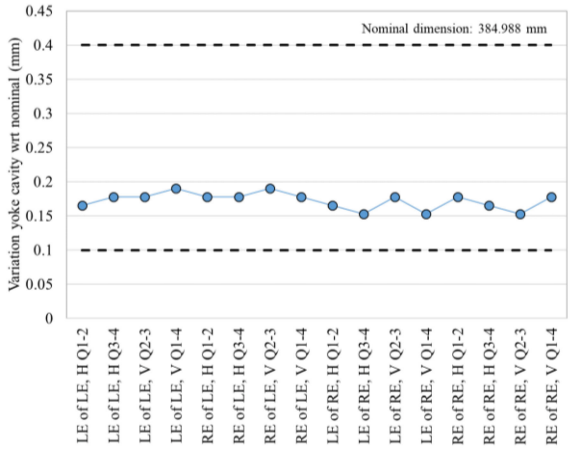

Fig. 5. Measurements of variation of yoke cavity dimension with respect to nominal size (384.99 mm): two horizontal (H) and two vertical (V) measurements taken on both side (LE and RE) of the two modules (LE and RE) in magnet MQXFA06; the dashed lines indicate the minimum and maximum values of the specifications.

- The shell strain in the axial direction after shell-yoke sub-assembly shall be within $-0.150/+0.050$ micro-strain

B. Yoke Cavity in Shell-Yoke Sub-Assembly

After the vertical loading operation is carried out for both the half-length shell-yoke modules, two horizontal and two vertical measurements of the yoke cavities on both extremities of the two modules are taken, for a total of 16 measurements (Fig. 5).

For the yoke cavity size after shell-yoke sub-assembly, the following specifications are set:

- The variation of yoke cavity dimension with respect to nominal shall be within $+0.100/+0.400$ mm.

IV. Coil-Pack Sub-Assembly

The assembly of the coil-pack sub-assembly (Fig. 2, center) takes place when four pad-collar stacks are bolted around the coils. In order to compensate for differences in coil sizes, both along the azimuthal and radial directions, polyimide shims are inserted on the mid-planes (in between the coils) and on the radial surfaces between the coil and the collar. The shim thicknesses are determined according to CMM measurements of each coil. Once the coil-pack is assembled, dimensional measurements are taken. The related specifications will be described in the next sub-sections.

A. Radial Contact Between Insulated Coil and Collars

In the nominal conditions, i.e., assuming all coils and collars have the nominal dimensions, the radial gap between the impregnated coil outer radius (113.376 mm) and the collar inner radius (114.000 mm), is 0.624 mm. This gap is supposed to be filled by layers of polyimide sheets (radial shims). However, since the beginning of the development of shell-based structures by LARP, it has become a common practice to remove 0.125 mm of insulation from the nominal radial shim in order to improve

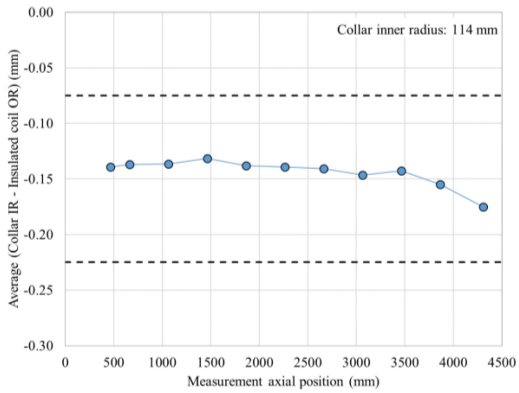

Fig. 6. Variation along the longitudinal direction of the gap between collars and insulated coils, considering for each z location the average among the four coils (from LE to RE); the dashed lines indicate the minimum and maximum values of the specifications.

the pre-load and stress distribution of the coil. This change was implemented for the first time in the LQ magnets, where it was noticed that the collar had the tendency to contact the coil predominantly on the pole area rather than on the coil outer radius [15]. This effect, called "LQ effect", resulted in excessive coil bending and a lower coil azimuthal pre-load. A significant improvement on the coil stress distribution was achieved by removing radial shims between coil and collar, therefore introducing a "radial gap" between the insulated coils and the collars. In fact, by removing insulation layers, the "insulated coil outer radius" is reduced. As a result, the collar, now featuring a larger radius than the coil, tends to push more towards the mid-plane (see a representation of this effect on Fig. 7 in [15]). A mechanical analysis demonstrating the effectiveness of the shim removal was presented in [16]. The same solution is adopted in MQXFA. As a result, the following specification is set:

- The variation along the longitudinal direction of the gap between collars and insulated coils, considering for each z location the average among the four coils, shall be -0.125 mm -0.100 / $+0.050$ mm.

In Fig. 6, the specifications of the radial gap are plotted together with the values obtained in the magnet MQXFA06. Each marker represents the average insulated coil to collar gap among the four coils, estimated using CMM measurements of the coil arc length, including mid-plane shims, taken on 11 longitudinal positions. The decreasing trend observed towards the RE is due to a reduction in azimuthal size measured in 3 out of the 4 MQXFA06 coils between the 3500 mm and 4500 mm axial positions.

B. Coil-Pack Sub-Assembly Dimensions

Once the bolting operation is completed, the coil pack vertical dimensions are measured on 11 longitudinal locations along the length. In each cross-section, two horizontal (Top and Bottom) and two vertical (Left and Right) dimensions are taken, as shown in the pictures inside Figs. 7 and 8.

Two parameters are monitored: 1) the *uniformity* of the vertical and horizontal dimensions along the z axis, given by the

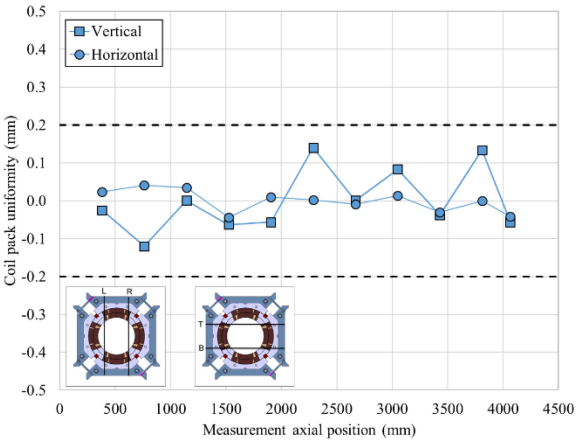

Fig. 7. Measured coil-pack vertical (horizontal) uniformity along the z axis (from LE to RE), given by the difference of the average of the Left (Top) and Right (Bottom) vertical (horizontal) dimensions in each cross-section with respect to the measured vertical (horizontal) average dimensions of the entire coil pack; the dashed lines indicate the minimum and maximum values of the specifications.

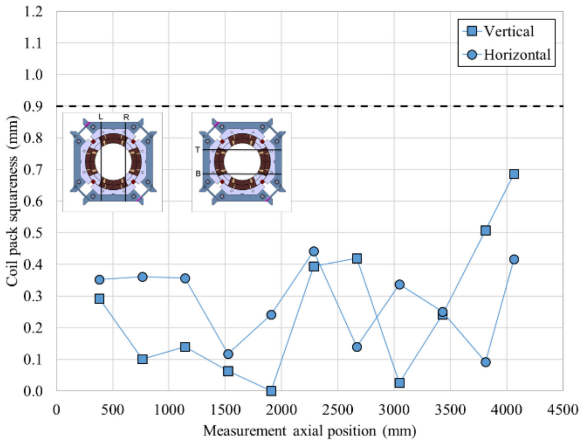

Fig. 8. Measured coil-pack squareness in the vertical (horizontal) direction along the z axis (from LE to RE), given by the absolute difference of the Left (Top) and Right (Bottom) vertical (horizontal) dimensions in each cross-section; the dashed lines indicate the minimum and maximum values of the specifications.

difference of the average of the L and R (T and B) vertical (horizontal) dimensions in each cross-section with respect to the measured vertical (horizontal) average dimension of the entire coil-pack; 2) the *squareness* in the vertical and horizontal directions along the z axis, given by the difference of the L and R (T and B) vertical (horizontal) dimensions in each cross-section.

For these two parameters the specifications are:

- The uniformity of the vertical and horizontal dimensions along the z axis shall be within ± 0.200 mm
- The squareness of the vertical and horizontal dimensions along the z axis shall be within $+0.900$ mm

C. Pole-Key Gap

In addition to the vertical and horizontal dimension of the coil-pack, the gap between the pole key and the collars, including the ground insulation, called the pole key gap (see picture in Fig. 9),

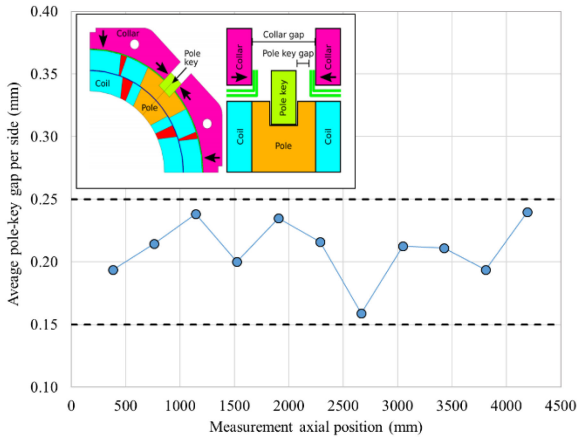

Fig. 9. Measured pole key gap per side in magnets MQXFA06: average among the four coils (from LE to RE); the dashed lines indicate the minimum and maximum values of the specifications.

is measured. According to the finite element computations [17], a gap of 0.200 mm per side at the end of coil-pack bolting closes at the end of the cool-down.

In this ideal scenario, from the room temperature pre-load operations to the end of the cool-down, no pre-load force generated by the bladders and the aluminum shell is intercepted by the pole key. At the same time, azimuthal alignment between collars and coil is achieved at 1.9 K.

The pole-key gap is measured on all the four coils and along the z axis at 11 longitudinal locations. Fig. 9 shows the average values and variations observed in MQXFA06. For the pole key gap, the following specifications are set:

- The average pole key gap (per side) among the four coils on each longitudinal location shall be $+0.200 \pm 0.050$ mm.

According to finite element computations, a ± 0.050 mm variation with the respect to the $+0.200$ mm target will not produce a relevant impact on coil pre-stress and alignment after cool-down.

V. Magnet Loading

The completion of the shell-yoke sub-assembly and of the coil-pack sub-assembly is followed by the assembly and pre-load of the full magnet. The coil-pack is slid inside the shell-yoke sub-assembly, and master keys and bladders are inserted in the slots between yoke and pads (see Fig. 2, right). A high-pressure pump is attached to the bladders on both ends of the magnet, and the axial loading system is attached to the axial rods to perform the axial pre-load operations. By inflating the bladders at progressively higher pressures, the load keys are shimmed to obtain the target strain on the shells and coils. In parallel, the axial rods are pre-tensioned.

A. Pre-Loading Sequence, Targets and Maximum Stress

For the pre-load operation sequence, the following specifications are set:

1. Pre-load axial rods with average to a measured of strain of $\sim 50\ \mu\varepsilon$

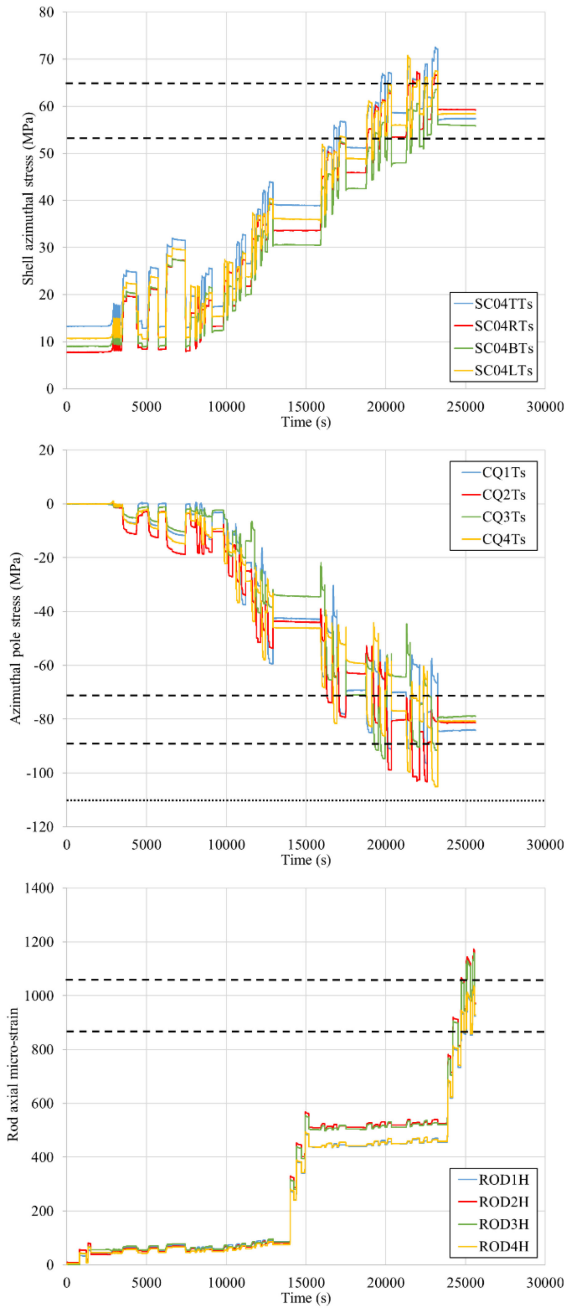

Fig. 10. Pre-load sequence of MQXFA06: shell azimuthal stress (top), coil azimuthal stress (center), rod axial strain (bottom); the dashed lines indicate the minimum and maximum values of the specifications, the dotted line indicates the specification of the maximum coil stress.

2. Apply 50% azimuthal pre-load
3. Apply 50% axial pre-load
4. Apply 100% azimuthal pre-load
5. Apply 100% axial pre-load

This pre-load sequence can be seen in Fig. 10, where the shell azimuthal stress (top), the coil pole azimuthal stress (center), and the rod strain (bottom) during MQXFA06 pre-loading are plotted: the coil and shell pre-loading via the bladder operation is executed in two steps, separated by a plateau (in correspondence of the 15000 s) where the first step of the axial loading is carried out. The second step of the axial loading is then executed at the end of the shell-coil loading.

The target pre-load levels for shells, coils and rods are chosen based on the experience of successful short and pre-series models, which is summarized in [3]. The specification for the room temperature pre-loads is set in order to achieve, after cool-down, an azimuthal pre-compression of 100-110 MPa in the coil pole and a total axial force provided by the four axial rods of 1.1 MN at 1.9 K. These values were chosen in particular accordingly to the ones applied in MQXFS4, which showed the best training performance among the short models. According to strain gauge data, this level of azimuthal pre-compression maintains during powering the coil in contact to the winding pole up to about 90% of the nominal current. Similarly, the axial force provided by the rod is equivalent to the electro-magnetic force acting on the coil ends at nominal current.

Therefore, the following specifications are set:

- The target average measured stress on coils, shells and rods at the end of the loading (after at least 24 h) shall be
- Shell average azimuthal stress: $+58 \pm 6$ MPa
- Coil (winding pole) average azimuthal stress: -80 ± 8 MPa
- Rod average strain: $+950 \pm 95$ $\mu\varepsilon$

In order to minimize the risk of permanent conductor degradation due to high stress during pre-load at room temperature, a maximum stress of -120 MPa in the coil has been established. The value was based on experience from LARP short model magnets (where the guideline was to minimize the pre-load given by bladders and maximize that provided by the cool-down of the aluminum shell). Moving from short models to long coils, a more conservative value was chosen to account for dimensional variations of coils. Therefore, for the maximum stress reached during the room temperature pre-load operations, the following specifications are set:

- During the entire pre-load operation, the maximum compression measured on each coil shall never exceed -110 MPa

An example of the coil stress measured during the bladder operations of MQXFA06 is shown in Fig. 10, center, with the dotted line indicating the maximum allowable stress.

However, as stated in Section II, the coil stress is measured only close to the RE, specifically at 3965 mm from LE. So, in order to estimate the stress in the coil along the longitudinal location, we rely on a sensitivity analysis of the coil and shell stress vs the load key thickness performed with 2D FE models and confirmed with strain data in short models (see [16]–[19]). The analysis suggests that the computed sensitivity of shell and coil stress to key thickness (which basically correspond to coil radial variations) is respectively 120 MPa/mm and -200 MPa/mm. In particular, according to the sensitivity analysis:

- $+0.100$ mm of coil outer radius increase
  - -20 MPa of coil stress variation
  - $+12$ MPa of shell stress variation
- $+0.100$ mm of total coil arc-length increase (0.050 per mid-plane)
  - -13 MPa of coil stress variation
  - $+8$ MPa of shell stress variation

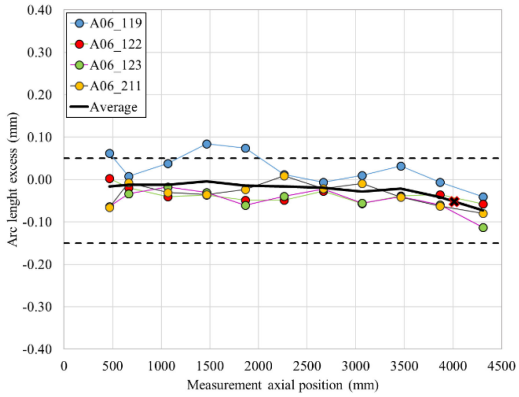

Fig. 11. Average shimmed coil size (arc length) for MQXFA06 (from LE to RE). The black cross marker indicates the location of the strain gauge station; the dashed lines indicate the minimum and maximum values of the specifications.

In order to minimize the variation of stress along the length, we define a target range of the average coil azimuthal size with respect to the size at the strain gauge station. The range is set based on the sensitivity analysis after coil shimming and assuming that only the average coil size plays a role in the coil stress.

For the maximum coil size (arc length) variation along the coil length, the following specifications are set:

- Average coil size (arc length) after shimming shall range within ± 100 µm with respect to average coil size measured in the strain gauge location.

A representation of this specification is shown in Fig. 11, where the average shimmed coil size (arc length) for MQXFA06 is plotted, and where the black cross marker indicates the location of the strain gauge station. The chosen range of ± 100 µm for the average coil size can be justified as follows: regarding the -80 ± 8 MPa specification for the average stress after bladder operation, a ± 100 µm average arc length variation with respect to the strain gauge location could results in a possible maximum average coil stress of $-88-(13)$ MPa $= -101$ MPa. This value was achieved in the successful short model MQXFS5 [3]. On the opposite extreme, the ± 100 µm average arc length variation could results in a coil pole pre-load as low as $-72+(13)$ MPa $= -59$ MPa, a value significantly higher than the one experienced on the successful magnet MQXFS6c [7]. For what concerns instead the -110 MPa specification for maximum compression measured on each coil during pre-load operations, a ± 100 µm average arc length variation with respect to the strain gauge location results in a possible maximum coil stress of $-110-(13)$ MPa $= -123$ MPa. This value would be marginally higher than the -120 MPa original LARP limit mentioned and still lower than the -140 MPa reached during bladder operation in the successful short model MQXFS5 [3].

VI. Conclusion and Future Plans

For the assembly and pre-load of the series MQXFA magnets for the AUP project a set of specifications were defined based on previous experience from the LARP project and the MQXF short model and prototype programs. The specifications focus on the dimensional measurements carried out on the sub-components of the magnet, like shell-yoke sub-assembly and coil-pack sub-assembly, and, in particular, on the pre-load of the superconducting coils: 1) the pre-load operation shall be conducted by applying in a progressive way both the axial and the azimuthal pre-load; 2) the average azimuthal coil pole pre-load shall be -80 ± 8 MPa; 3) the coil peak stress shall be kept below -110 MPa during all pre-loading operations; 4) the coil average size variation shall be kept between ± 100 µm to keep the coil stress variation within ± 13 MPa.

References

[1] G. Ambrosio *et al.*, "Lessons learned from the prototypes of the MQXFA low-beta quadrupoles for HL-LHC and status of production in the us," *IEEE Trans. Appl. Supercond.*, vol. 31, no. 5, Aug. 2021, Art. no. 4001105.

[2] O. Brüning and L. Rossi,"The high luminosity large hadron collider," World Scientific, Oct. 2015.

[3] E. Todesco *et al.*, "The high luminosity LHC interaction region magnets towards series production," *Supercond. Sci. Technol.*, vol. 34, 2021, Art. no. 053001.

[4] P. Ferracin *et al.*, "The HL-LHC low-b quadrupole magnet MQXF: From short model to long prototype," *IEEE Trans. Appl. Supercond.*, vol. 29, no. 5, Aug. 2019, Art. no. 4001309.

[5] S. I. Bermudez *et al.*, "Progress in the development of the nb_3Sn MQXFB quadrupole for the hilumi upgrade of the LHC," *IEEE Trans. Appl. Supercond.*, vol. 31, no. 5, Aug. 2021, Art. no. 4002007.

[6] F. J. Mangiarotti *et al.*, "Powering performance and endurance beyond design limits of HL-LHC low-beta quadrupole model magnets," *IEEE Trans. Appl. Supercond.*, vol. 31, no. 5, Aug. 2021, Art. no. 4000805.

[7] S. I. Bermudez *et al.*, "Performance of a MQXF nb_3Sn quadrupole under different stress level," *IEEE Trans. Appl. Supercond.*, to be published.

[8] J. F. Muratore *et al.*, "Test results of the first two full-length prototype quadrupole magnets for the LHC hi-lumi upgrade," *IEEE Trans. Appl. Supercond.*, vol. 30, no. 4, Jun. 2020, Art. no. 4004205.

[9] J. F. Muratore *et al.*, "Test results of the first pre-series quadrupole magnets for the LHC hi-lumi upgrade," *IEEE Trans. Appl. Supercond.*, vol. 31, no. 5, Aug. 2021, Art. no. 4001804.

[10] F. J. Mangiarotti *et al.*, "Power test of the first two MQXFB quadrupole magnets built at CERN for the HL-LHC low-beta insertion," *IEEE Trans. Appl. Supercond.*, to be published.

[11] S. Gourlay *et al.*, "Magnet R&D for the US LHC research accelerator program (LARP)," *IEEE Trans. Appl. Supercond.*, vol. 16, no. 2, pp. 324–327, Jun. 2006.

[12] P. Ferracin, "LARP nb_3Sn quadrupole magnets for the LHC luminosity upgrade," in *Proc. AIP Conf.*, 2010, pp. 1291–1300, vol. 1218.

[13] D. W. Cheng *et al.*, "Fabrication and assembly performance of the first 4.2 m MQXFA magnet and mechanical model for the hi-lumi LHC upgrade," *IEEE Trans. Appl. Supercond.*, vol. 28, no. 3, Apr. 2018, Art. no. 4006207.

[14] G. Vallone *et al.*, "Mechanical performance of short models for MQXF, the nb_3Sn Low-β quadrupole for the hi-lumi LHC," *IEEE Trans. Appl. Supercond.*, vol. 27, no. 4, Jun. 2017, Art. no. 4002906.

[15] P. Ferracin *et al.*, "Mechanical performance of the LARP nb_3Sn quadrupole magnet LQS01," *IEEE Trans. Appl. Supercond.*, vol. 21, no. 3, Jun. 2011, Art. no. 1683.

[16] E. Takala *et al.*, "Preload characterization of short models of MQXF the Nb3Sn low-β quadrupole for the hi-lumi LHC," *IEEE Trans. Appl. Supercond.*, vol. 30, no. 4, Jun. 2020, Art. no. 4002806.

[17] G. Vallone *et al.*, "Mechanical analysis of the short model magnets for the Nb3Sn low-β quadrupole MQXF," *IEEE Trans. Appl. Supercond.*, vol. 28, no. 3, Apr. 2018, Art. no. 4003106.

[18] G. Vallone *et al.*, "Summary of the mechanical performances of the 1.5 m long models of the nb_3Sn low-β quadrupole MQXF," *IEEE Trans. Appl. Supercond.*, vol. 29, no. 5, Aug. 2019, Art. no. 4002805.

[19] E. Takala *et al.*, "On the mechanics of MQXFB - the low-beta quadrupole for the HL-LHC," *Supercond. Sci. Technol.*, vol. 34, 2021, Art. no. 095002.